Erschienen in: Advanced Materials ; 29 (2017), 2. - 1603356
https://doi.org/10.1002/adma.201603356

Functional Gradient Inverse Opal Carbon Monoliths with Directional and Multinary Porosity

*Mengdi Chen, Kay Hagedorn, Helmut Cölfen, and Sebastian Polarz**

Porous solids represent a class of materials of extreme value documented by a plethora of properties and applications in industry and modern research.[1] They find use in areas like adsorption, separation, catalysis, sensing, and lately also in energy-storage applications. Enormous work has been invested in controlling pore-sizes and chemical functionalities in porous materials.[2]

A particularly interesting scenario is, if one could achieve a hierarchical porous structure.[3] The interested reader is referred to the seminal work published by Li et al. in 2012, for instance.[4] Reports addressing the preparation and benefits of materials with bimodal pore-size distribution deserve attention.[5] A less noted, distinct element of hierarchy is the occurrence of specific gradients over changing dimensions. In so-called functional gradient materials (FGMs),[6] a sharp boundary is replaced by a gradient at the microstructural level. This causes a smooth transition from one property to the next, and it is expected that such a special character enables materials to perform more advanced tasks. On FGMs with a gradient in pore-size, the number of examples is extremely small. In 2015 our group presented macroporous organosilica aerogels having gradient porosity, but without showing any application.[7] A nice paper demonstrating the benefits of a gradient pore structure in the solid-oxide fuel cell was published by Brandon and Brett in 2006.[8] Luo et al. presented an impressive study in 2015.[9] The authors describe a macroporous hydrogel composed of *N*-isopropylacrylamide prepared by hydrothermal synthesis. It could be shown that programmable locomotion became possible owing to the gradient porosity. However, in all the latter cases pore-sizes were in the range ≈ 1 μm, the pore-size distribution function was broad, and the materials were not electrically conducting. There is a demand for gradient porous materials with nanoscaled pores and much more defined pore-size distribution, preferentially with conducting framework for applications in energy-storage, electrocatalysis, thermoelectrics, etc.

Among the different classes of electrically conducting, porous materials carbon has received a position in the recent spotlight.[10] This is first and foremost a result of the synergy resulting from high surface area and the unique electronic and redox-properties of graphitic variants of carbon.[11] A powerful method for preparing porous carbon materials is the use of templates in combination with different carbon precursors.[10a,12] A reliable approach is the resorcinol-formaldehyde (RF) route.[13] First one prepares a cross-linked hydrogel, which after drying is thermally converted to carbon.[14] As templates one has often used latex particles, for example for preparing inverted carbon opals. A nice review has been published by Smarsly and co-workers in 2012.[15] There also have been some reports on porous carbon materials with bimodal pore-structure.[5c,16] However, to the best of our knowledge there does not yet exist a carbon material with a gradient pore-structure.

The major reason for the latter is that suitable templates, which present gradient porous materials themselves, are not readily available. Recently we studied the sedimentation behavior of dispersions containing a binary mixture of spherical polystyrene–polystyrenesulfonate (PS) particles in water using analytical ultracentrifugation.[17] We found not only that unusual, ordered aggregates could be obtained, but separation of particles has been controlled to such an extent that a gradient emerged (see Figure S-1 in the Supporting Information). Therefore, in the current paper we explore, if the described methodology can be used for preparing a carbon material with a defined gradient pore-structure.

Our first idea was to use monoliths containing the described gradient structure of the PS spheres[17a] as a template for the infiltration of resorcinol-formaldehyde sol as a source for carbon. After polycondensation, drying and carbonization the resulting material was analyzed. Unfortunately, we noted macroscopic and microscopic cracking, and as a result we only got irregularly shaped pieces (see Figure S-2 in the Supporting Information). Using scanning electron microscopy (SEM) one finds the preparation of an inverted, macroporous materials has essentially worked. However, there are many cracks and undesired voids. Further, we also saw that it is difficult to assure that also the internal regions of the monolith are filled with carbon. Therefore, the "direct infiltration approach" was not pursued further. The quality of the material was too low. Also in the literature,[18] monolithic porous carbon materials (PCMs) could only be prepared containing a substantial amount of defects and cracks. A method which could achieve PCMs with limited cracks and uniform porosity remains to be developed.

Our next idea was to assemble the PS spheres directly in the RF sol and finish assembly before gelation takes place. We used a so-called swing-out centrifuge rotor, which assures a horizontal centrifugal force parallel to the centrifuge tube (see **Scheme 1**). Because the density of the RF sol is higher than that of the PS spheres, rather than sedimentation the application of centrifuge force induces flotation of the polymeric particles in opposite direction.

Before we explore the possibility for preparing gradient porous carbon materials using a bimodal mixture of PS spheres as templating entities, it is important to prove the general feasibility of the method. Therefore, the monodisperse system

M. Chen, K. Hagedorn, Prof. H. Cölfen, Prof. S. Polarz
Department of Chemistry
University of Konstanz
Universitätsstr. 10, 78457 Konstanz, Germany
E-mail: sebastian.polarz@uni-konstanz.de

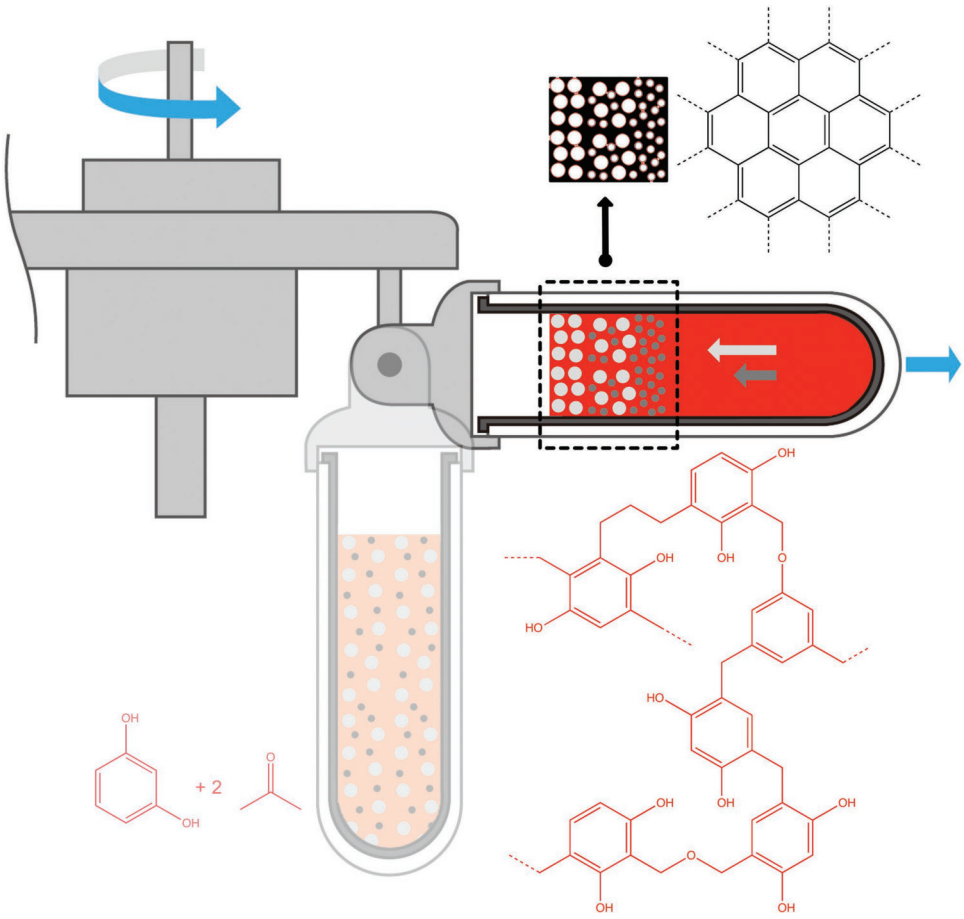

Scheme 1. Swing out rotor filled with a colloidal solution of PS spheres (eventually of different size) plotted as gray circles and a resorcinol formaldehyde sol (salmon color). The rotation and the direction of the gravitational field are marked by blue arrows. Flotation of the PS spheres (different flotation rates marked by gray arrows) and polycondensation of the RF gel (red) take place simultaneously to each other. Finally, a monolithic RF/PS composite gel can be separated and is converted to porous sp^2-hybridized carbon (black) finally with gradient pore-structure.

is discussed first. Macroscopic and crack-free monoliths of the RF/PS nanocomposite can be obtained. A photographic image and extra analytical data are given in Figure S-3 in the Supporting Information. Thermal treatment then induces the transformation to carbon at T = 437 °C according to thermogravimetric analysis given in Figure S-4 in the Supporting Information. The successful conversion was checked by FT-Raman spectroscopy, powder X-ray diffraction (PXRD) and Fourier transform infrared spectroscopy (Figure S-4, Supporting Information). The Raman spectrum displays two broad bands at 1298 and 1607 cm^{-1}, which is characteristic for disordered carbon with predominantly sp^2 hybridization.[19,20] The latter is supported by PXRD. Only two diffraction peaks are seen (2θ = 25, 44°) and can be assigned to the (002) and (101) planes of graphite. However, the large width of the signals ($\Delta 2\theta_{002}$ = 7.8°; full width at half maximum) processed using Scherrers equation correlate to a domain size in c-direction of less than 2 nm. This agrees with a highly disordered, turbostratic carbon. However, it is more important to note that crack-free monoliths can be obtained even after the high-T carbonization step (see Figure S-3a in the Supporting Information). Compared to the RF/PS nanocomposite it has shrunk in size/volume because of the loss of H_2O and densification caused by progressing C—C bond formation (see Scheme 1). Using SEM one can show the PCMs are crack-free on the micro- and nanoscale (**Figure 1**a–c).

Besides the fundamental difference in synthesis approach compared to the classical infiltration described before, from the SEM images we learn one important reason for the superior homogeneity. When using ultracentrifugation for the assembly of the PS spheres there is a high tendency for forming a glassy state, which then is replicated as a porous carbon structure. The PS spheres pack dense, and a certain degree of short-range order, but there is no long-range periodicity as in a crystalline lattice (e.g., face centered cubic, fcc). So, domains and grain boundaries are missing. It can also be shown the large pores are interconnected by small pores (see Figure S-5 in the Supporting Information). The PCMs possess a high accessible pore volume (e.g., V_{pore} = 0.87 $cm^3\ g^{-1}$) and high accessible specific surface area (e.g., A_{spec} = 770 $m^2\ g^{-1}$) determined from N_2 physisorption isotherms shown in Figure S-6 in the Supporting Information.

It is important to note that homogeneous materials with a dense packing of pores can only be obtained for sufficiently high concentrations of resorcinol/formaldehyde in the aqueous

dispersion (see the Experimental Section). At concentrations too low one can see that domains of pores created by the PS spheres as templates are separated by larger, irregular voids; see SEM data in Figure S-7 in the Supporting Information. Depending on the size of the PS spheres also the pore-size of the carbon material can be tuned (Figure 1d–f). The resulting pores are smaller than the diameter of the PS spheres (e.g., D_{PS} = 110, 250, 500 nm (D_{pore} = 40, 180, 420 nm). This caused by the described shrinking in due course of carbonization. Because the resulting pore size depends linearly on D_{PS} (Figure S-6b, Supporting Information), there is full control over the porosity of the porous carbon material.

Because we have mastered the in situ PS assembly/RF gel formation and its transformation into PCMs with homogeneous porosity, we will now use a mixture of PS template particles ultimately aiming at creating gradient porosity. The sedimentation behavior of binary latex dispersions studied by analytical ultracentrifugation and focusing on the emergence of binary lattice structures is described in detail in ref. [17a]. The way the spheres separate is determined from the control of several parameters like centrifugation force (F), centrifugation time (t), column length (L), total volume fraction of particles (Φ), and number ratio of two particles ($N = N_{PS1}/N_{PS2}$). Through the characterization of analytical ultracentrifugation, the number of variable parameters can be reduced to two. The systems in the current work is more complicated, because due to the RF sol there is flotation of PS spheres rather than sedimentation (Scheme 1) and the solvent viscosity changes with time. Therefore, we keep centrifugation conditions fixed but play subtly with the number ratio of the two particles to reach different separation scenarios. One scenario is the large pores are randomly scattered in the matrix of the small pores (**Figure 2**a). Again the advantage of the glassy state can be appreciated, because one can conclude the presence of the larger PS spheres (→ large pores) does not disturb packing the small PS spheres (→ small pores). The other extreme is given by sharp separation between small and large PS spheres. As a result, one gets a porous carbon material with a distinct boundary between large and small pores shown in Figure 2b.

Now it should be possible to achieve monoliths with gradient pore systems for a scenario between full mixing and sharp separation. First, we tested a binary dispersion of PS spheres (D_{PS} = 250, 500 nm) as templates. Indeed, one can now prepare a porous carbon material with a directional change of the density of one type of pore as shown in Figure S-10 in the Supporting Information (PCM-6). Besides, one can even use a ternary mixture of template particles (D_{PS} = 110, 250, 500 nm) as shown in **Figure 3** (PCM-7). At the top one sees a porous matrix only with 40 nm pores, followed by a region with some, randomly distributed 180 nm pores. The density of the 180 nm pores then becomes higher, till eventually 40 nm pores vanish, and at the same time one can observe the occurrence of 420 nm large pores.

The next important question is, if the gradient porosity leads to some profitable properties. Diffusive and convective transport phenomena are always important subjects in porous media. A concrete example of prevailing importance is the lithium-oxygen (Li-O_2) battery ($2Li + O_2 \leftrightarrow Li_2O_2$, E^0 = 2.96 V vs Li/Li^+).[21] The role of porosity for the Li-O_2 battery was subject of several papers.[18b,22] Olivares-Marín et al.[23] studied pore-size

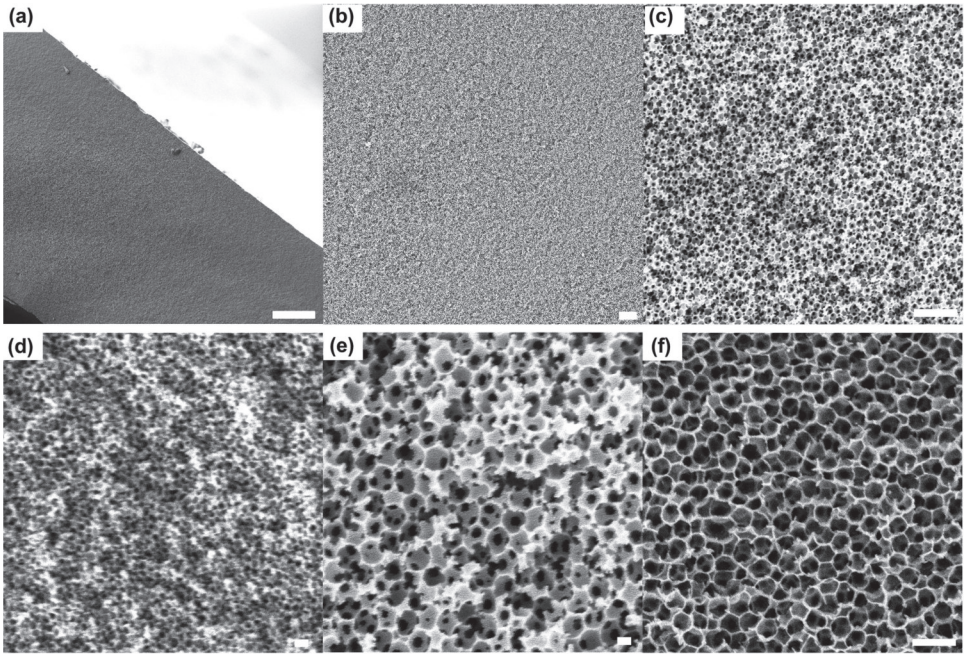

Figure 1. SEM micrographs taken at different magnification for one porous carbon material showing the crack-free, homogeneous character of the monoliths; a) scale bar = 100 µm, b) scale bar = 2 µm, c) scale bar = 1 µm. SEM micrographs of PCMs with different pore-size controlled by means of the size of the latex particles as templates; d) D_{pore} = 40 nm (PCM-1), scale bar = 100 nm; e) D_{pore} = 180 nm (PCM-2), scale bar = 100 nm; D_{pore} = 420 nm (PCM-3), scale bar = 1000 nm.

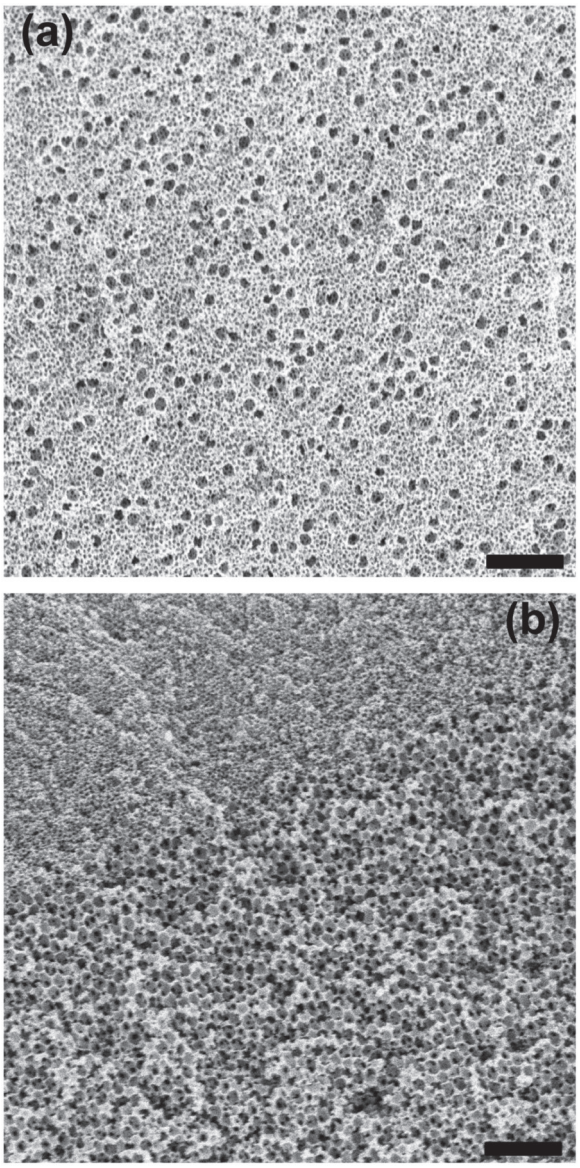

Figure 2. SEM micrographs for the scenario of a carbon material with bimodal porosity and random mixing of two pore-sizes a) PCM-4, scale bar ≅ 1 µm; see also Figure S-8 in the Supporting Information. b) Pore-system for the sharp separation scenario (PCM-5), scale bar ≅ 1 µm; see also Figure S-9 in the Supporting Information for images taken at alternative magnifications. Binary mixture PS spheres (D_{PS} = 110, 250 nm) used as templates.

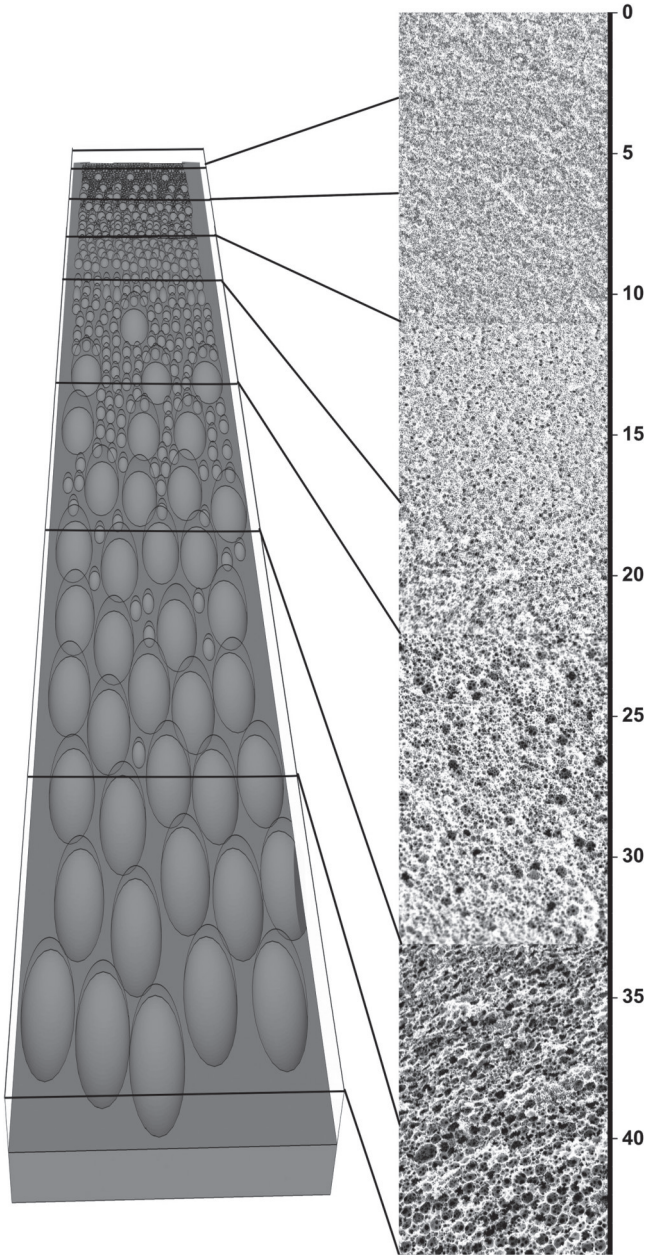

Figure 3. 4× consecutive SEM micrographs of a porous carbon with ternary gradient porosity (PCM-7); scale bar (plotted as a y-axis) units in µm. And a scheme pointing out the gradient porosity.

effects of the porous carbon cathode and found that smaller macropores favor charge–discharge reversibility while large macropores contribute to a large capacity. Using theoretical methods Li and Faghri[24] developed a 2D model to simulate the mass transfer characteristics in the cathode of the Li-O_2 battery. They predicted the capacity of a Li-O_2 battery could be increased by adopting a unique designed carbon cathode with a non-uniform porosity distribution and an increasing porosity at the electrolyte/O_2 interface. It can be concluded the carbon materials described herein with gradient porosity are promising candidates for testing their performance in the Li-O_2 battery.

Four different porous carbon monoliths (PCMs-1-3, 6) were tested (see **Figure 4**). One side of the porous carbon cathode faces the O_2 environment and the other side faces the separator saturated with electrolyte (Figure 4a). Three materials are monomodal in pore-size ($D_{PM\text{-}1,2,3}$ = 40, 180, 420 nm; see also Figure 1d–f)) and one material (PCM-6) possesses a bimodal gradient pore-system (see Figure 4b and Figure S-10 in the Supporting Information). The material shown in Figure 2b with a distinct boundary would also be very interesting, but unfortunately the irregular shape of the monolith after carbonization hampered performing the electrochemical experiments. The

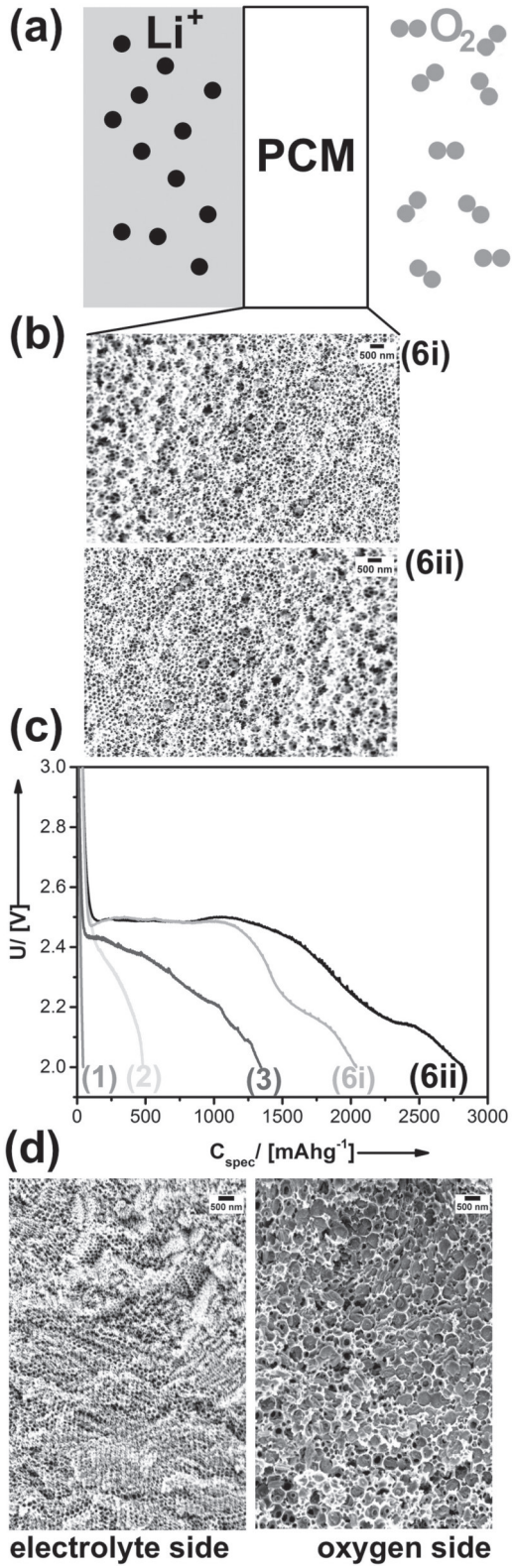

Figure 4. a) Position of the PCM monolith in the Li-O_2 battery testing setup. b) SEM image of PCM-6 and the two alternative orientations. c) Li-O_2 electrochemical discharge curves. d) SEM investigation of PCM-6ii after charging/cycling.

Li-O_2 cells were assembled using the PCM materials in their monolithic form so the direction of the gradient is defined. Cycling performance was measured (data given in Figure S-11 in the Supporting Information) and the specific capacity C_{spec} was obtained from discharge measurements (Figure 4c). The monolithic shape was preserved during the preparation of Li-O_2 cell as well as in the process of charge–discharge cycle of the batteries.

PCM-1 with small pores is inferior, and the performance becomes better with increasing pore-size, agreeing with reports from others.[23,25] This behavior can be understood considering the actual capacity of the Li-O_2 battery is limited by the formation rate of Li_2O_2 during discharge.[21a] It is interesting to note the SEM images of the materials after charging. It can be seen that significant amount of Li_2O_2 is present in PCM-3 with larger pores (see Figure S-12a in the Supporting Information). In comparison, for PCM-2 Li_2O_2 has only formed at the surface of the electrode and the pore-system is almost empty (see Figure S-12b in the Supporting Information). This explains the low capacity of PCM-2. The latter result shows the Li_2O_2 deposit can also be a problem. Once the pore entrances are blocked mass transport through the electrode is aggravated and this impedes to reach the maximum capacity.

Therefore, we expect that a material with two different pores (PCM-6) could be superior because one type of pore (180 nm) will be not filled so quickly granting prolonged mass transport, and the other type of pore (420 nm) will contribute to capacity via Li_2O_2 deposition. From Figure 4c one can see that this is the case. However, it is more interesting to note the capacity depends on how PCM-6 is positioned. Because of its internal directionality sample PCM-6 can either be placed the smaller pores facing the O_2 environment (case i) or vice versa (case ii). Clearly PMC-6ii has an even higher capacity than PCM-6i. Considering the previous arguments this behavior can be understood. When the smaller pores face the oxygen side, filling of the material with Li_2O_2 is still only partial (see Figure S-13a in the Supporting Information). However, when the large pores are facing the oxygen side one can see the pores are filled homogeneously with Li_2O_2 indicating that a large fraction of the surface of the porous material has contributed to the electrochemical reaction (see Figure 4d). The smaller pores in the gradient zone and those pointing to the electrolyte remain unfilled, and this secures mass transport in the electrode. As a result, PCM-6 is the material with the best performance in the Li-O_2 cell shown here. Compared to reports in the literature,[26] further development is needed to reach maximum capacities.

We could show that porous carbon monoliths with a crack-free structure could not be obtained using a classical template infiltration route. However, the in situ assembly of polystyrene spheres (as templates) and a resorcinol formaldehyde sol (as a carbon precursor) using ultracentrifugation leads to success. Controlling the flotation of differently sized PS spheres, also, enables to prepare carbon materials with bimodal or even trimodal porosity organized either as a random distribution, phase-separated or supremely as a gradient. The resulting carbon monoliths with gradient porosity were tested as electrodes in the Li-O_2 cell, and it was proved that not only the

gradient structure influences the performance of the cell, but also the direction of the gradient is of crucial importance.

Experimental Section

Experimental details are given in the Supporting Information.

Acknowledgements

M.C. was funded by a Chinese Scholarship Council stipend. K.H. was funded by the Carl-Zeiss foundation (REFINE research initiative).

[1] a) M. E. Davis, *Nature* **2002**, *417*, 813; b) S. Horike, S. Shimomura, S. Kitagawa, *Nat. Chem.* **2009**, *1*, 695; c) K. Ariga, A. Vinu, Y. Yamauchi, Q. M. Ji, J. P. Hill, *Bull. Chem. Soc. Jpn.* **2012**, *85*, 1.
[2] a) C. Sanchez, P. Belleville, M. Popall, L. Nicole, *Chem. Soc. Rev.* **2011**, *40*, 696; b) A. H. Lu, F. Schüth, *Adv. Mater.* **2006**, *18*, 1793.
[3] a) E. Munch, M. E. Launey, D. H. Alsem, E. Saiz, A. P. Tomsia, R. O. Ritchie, *Science* **2008**, *322*, 1516; b) D. W. Wang, F. Li, M. Liu, G. Q. Lu, H. M. Cheng, *Angew. Chem. Int. Ed.* **2009**, *48*, 1525.
[4] Y. Li, Z. Y. Fu, B. L. Su, *Adv. Funct. Mater.* **2012**, *22*, 4634.
[5] a) T. K. Maji, R. Matsuda, S. Kitagawa, *Nat. Mater.* **2007**, *6*, 142; b) M. Antonietti, B. Berton, C. Göltner, H. P. Hentze, *Adv. Mater.* **1998**, *10*, 154; c) A. H. Lu, W. Schmidt, B. Spliethoff, F. Schüth, *Adv. Mater.* **2003**, *15*, 1602.
[6] B. H. Rabin, I. Shiota, *MRS Bull.* **1995**, *20*, 14.
[7] A. Schachtschneider, M. Wessig, M. Spitzbarth, A. Donner, C. Fischer, M. Drescher, S. Polarz, *Angew. Chem. Int. Ed.* **2015**, *54*, 10465.
[8] N. P. Brandon, D. J. Brett, *Philos. Trans. R. Soc. A* **2006**, *364*, 147.
[9] R. Luo, J. Wu, N. D. Dinh, C. H. Chen, *Adv. Funct. Mater.* **2015**, *25*, 7272.
[10] a) J. Lee, J. Kim, T. Hyeon, *Adv. Mater.* **2006**, *18*, 2073; b) A. Stein, Z. Y. Wang, M. A. Fierke, *Adv. Mater.* **2009**, *21*, 265.
[11] Y. P. Zhai, Y. Q. Dou, D. Y. Zhao, P. F. Fulvio, R. T. Mayes, S. Dai, *Adv. Mater.* **2011**, *23*, 4828.
[12] B. Hu, K. Wang, L. H. Wu, S. H. Yu, M. Antonietti, M. M. Titirici, *Adv. Mater.* **2010**, *22*, 813.
[13] C. Moreno-Castilla, F. J. Maldonado-Hodar, *Carbon* **2005**, *43*, 455.
[14] S. A. Al-Muhtaseb, J. A. Ritter, *Adv. Mater.* **2003**, *15*, 101.
[15] L. Chuenchom, R. Kraehnert, B. M. Smarsly, *Soft Matter* **2012**, *8*, 10801.
[16] Z. Y. Yuan, B. L. Su, *J. Mater. Chem.* **2006**, *16*, 663.
[17] a) M. Chen, H. Cölfen, S. Polarz, *ACS Nano* **2015**, *9*, 6944; b) M. Chen, H. Cölfen, S. Polarz, *Z. Naturforsch. B: J. Chem. Sci.* **2013**, *68*, 103.
[18] a) S. Liu, Z. Wang, C. Yu, Z. Zhao, X. Fan, Z. Ling, J. Qiu, *J. Mater. Chem. A* **2013**, *1*, 12033; b) W. B. Luo, S. L. Chou, J. Z. Wang, Y. C. Zhai, H. K. Liu, *Small* **2015**, *11*, 2817; c) K. T. Lee, J. C. Lytle, N. S. Ergang, S. M. Oh, A. Stein, *Adv. Funct. Mater.* **2005**, *15*, 547.
[19] M. A. Pimenta, G. Dresselhaus, M. S. Dresselhaus, L. G. Cancado, A. Jorio, R. Saito, *Phys. Chem. Chem. Phys.* **2007**, *9*, 1276.
[20] C. SekharáRout, *Chem. Commun.* **2008**, *44*, 5155.
[21] a) Z. Peng, S. A. Freunberger, Y. Chen, P. G. Bruce, *Science* **2012**, *337*, 563; b) Z. Jian, P. Liu, F. Li, P. He, X. Guo, M. Chen, H. Zhou, *Angew. Chem. Int. Ed.* **2014**, *53*, 442.
[22] a) Z. Guo, D. Zhou, X. Dong, Z. Qiu, Y. Wang, Y. Xia, *Adv. Mater.* **2013**, *25*, 5668; b) Z. Zhang, J. Bao, C. He, Y. Chen, J. Wei, Z. Zhou, *Adv. Funct. Mater.* **2014**, *24*, 6826.
[23] M. Olivares-Marín, P. Palomino, J. M. Amarilla, E. Enciso, D. Tonti, *J. Mater. Chem. A* **2013**, *1*, 14270.
[24] X. Li, A. Faghri, *J. Electrochem. Soc.* **2012**, *159*, A1747.
[25] N. Ding, S. W. Chien, T. A. Hor, R. Lum, Y. Zong, Z. Liu, *J. Mater. Chem. A* **2014**, *2*, 12433.
[26] B. Sun, S. Q. Chen, H. Liu, G. X. Wang, *Adv. Funct. Mater.* **2015**, *25*, 4436.